

to the grating. The first-order diffracted beams leave the grating (G) at angles θ_1 and θ_2 given by the following relations:

$$\frac{\sin \theta_1}{\lambda_1} = \frac{\sin \theta_2}{\lambda_2} = F,$$

where $f_2\lambda_2 = f_1\lambda_1 =$ velocity of light and F = spatial frequency of the grating. In any plane parallel to the grating (G), the interference between a beam normal to the plane and the corresponding first-order diffracted beam gives fringes of spatial frequency F . This means that the average carrier frequency of the hologram recording is independent of the temporal frequency of the light. Thus, when one reconstructs a doubly exposed hologram of an object wavefront, an object ray normal to the hologram will be reconstructed in the same direction independent of its initial temporal frequency. Thus, the two coherent images reconstructed will be aligned and interfere very well if a viewing system with sufficiently large depth-of-field is used.

Shown in Fig. 2 is a contour map of a quarter made using the setup depicted in Fig. 1. The wavelengths used were 6118 Å and 6328 Å from a He:Ne gas laser; the contouring interval is roughly 9 μ . In addition to the simplicity of this technique, one can list the advantages: (1) path length adjustments for coherence requirements are made with much greater ease, which may be especially important for pulsed laser applications; (2) the holograms often can be reconstructed in white light; and (3) the method produces higher quality contour maps due largely to improved fringe localization.

Various explanations for the fringe localization problem in the old method are being investigated; aberrations introduced by the beam splitter and the telescope seem to be the most likely cause of this problem.

This work was supported by the U.S. Army Materials and Mechanics Research Center, Watertown, Massachusetts under contract number DAAG46-69-C-0017.

References

1. K. A. Haines and B. P. Hildebrand, *J. Opt. Soc. Amer.* **57**, 155 (1967).
2. B. P. Hildebrand, "A General Analysis of Contour Holography," Willow Run Technical Report 7421-33-T, Institute of Science and Technology, The University of Michigan, February 1968.
3. J. S. Zelenka and J. R. Varner, *Appl. Opt.* **7**, 2107 (1968).

Measurements of Photon Correlations in a Two Mode Laser Beam

F. Tittel, J. Klebba, and F. Davidson

F. Tittel and J. Klebba are with EE Department, Rice University, Houston, Texas 77001; F. Davidson is with EE Department, Johns Hopkins University, Baltimore, Maryland 21218.

Received 30 July 1970.

This Letter reports the results of measurements of the irradiance auto correlation function of a 6328-Å He:Ne gas laser operating in two independent axial modes. The measurements were made with the use of time-to-amplitude converter techniques¹ developed for the experimental determination of irradiance correlation functions. The advantages and limitations of this type of time domain measurement will be compared with those of the more conventional frequency domain measurements employing a scanning Fabry-Perot interferometer or an rf spectrum analyzer.

Irradiance auto correlation functions of the type $\langle \hat{I}(x,t)\hat{I}(x,t+\tau) \rangle$ have been calculated by several authors^{2,3} for the optical field produced by a laser operating in two independent axial modes. The colons denote that operators used to express the irradiance at point x , time t appear in normal order and the angular brackets indicate an ensemble average over all realizations of field irradiance. The irradiance correlation function of a laser operating in two axial modes of identical polarization and constant amplitude is given by:

$$\langle \hat{I}(x,t)\hat{I}(x,t+\tau) \rangle = \langle I(x) \rangle^2 [1 + \frac{1}{2}f(\tau) \cos(\omega_2 - \omega_1)\tau], \quad (1)$$

where $\langle I(x) \rangle$ = mean laser irradiance and ω_j = center angular frequency of the j^{th} mode. Now let us consider the following cases:

- (1) if the two modes are phase locked $f(\tau) = 1$;
- (2) if the two modes oscillate independently, are of equal strength and their phase undergo a random walk type of diffusion:⁴

$$f(\tau) = \exp \left[-\frac{1}{2} \sum_{j=1}^2 D_j |\tau| \right]$$

where D_j is the phase diffusion constant of the j^{th} mode, and is equal to 2π times the linewidth of the j^{th} mode;

- (3) if the two equal amplitude laser modes operate in some intermediate regime where they are neither phase locked nor completely independent;

$$f(\tau) = \langle \cos\{\Phi_2(t+\tau) - \Phi_2(t)\} - \{\Phi_1(t+\tau) - \Phi_1(t)\} \rangle,$$

where $\Phi_1(t)$, $\Phi_2(t)$ denote the phases of the two modes.

In principle, a detailed knowledge of $f(\tau)$ as a function of τ can then be used to distinguish the three cases. As the number of axial modes present in the beam increases, the irradiance auto-correlation function becomes more complex. For the case of three independent equal strength modes of the same polarization, equal adjacent mode spacing and equal mode linewidth,

$$\langle \hat{I}(x,t)\hat{I}(x,t+\tau) \rangle = \langle I(x) \rangle^2 [1 + (2/9)e^{-D|\tau|} \times \cos\Delta\omega\tau + (1/9)e^{-D|\tau|} \cos 2\Delta\omega\tau]. \quad (2)$$

In the limit as the number of modes present in the laser beam becomes infinite, $\langle \hat{I}(x,t)\hat{I}(x,t+\tau) \rangle$ becomes $\langle I(t) \rangle^2 [1 + |\gamma(\tau)|^2]$, where $\gamma(\tau)$ is the second order field strength correlation function.⁵ $|\gamma(\tau)|$ tends to zero for $\tau \neq 0$, with $|\gamma(0)| = 1$ as the number of laser modes becomes infinite.

The apparatus shown in Fig. 1 was used to measure the irradiance auto correlation function of a Spectra Physics Model 120 He:Ne gas laser operating in two independent axial modes. The mode structure of the laser was constantly monitored during the course of the measurements. Pulses from the individual photodetectors were amplified and standardized by the discriminators. The standardized pulses were then fed to the start and stop inputs of a time-to-amplitude converter (TAC). The TAC output pulses were then stored in one of the channels of a 512 channel pulse height analyzer. The height of each TAC output

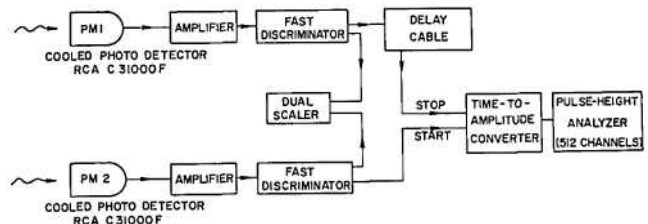


Fig. 1. Experimental arrangement for intensity correlation measurements of optical radiation fields.

pulse is linearly proportional to the difference in arrival times of the start and stop input photodetector pulses. A delay cable was inserted before the stop input of the TAC so that simultaneously detected photons would be recorded by TAC conversions of other than zero pulse height. The pulse height analyzer was allowed to accumulate TAC output pulses only when the laser mode amplitudes were within 20% of being equal.

The rate, $R(\tau)$, at which the TAC produces conversions that correspond to two photons absorbed τ seconds apart by the two photodetectors has been related to the irradiance correlation function in Ref. 6. The result of the analysis is that the component of the normalized irradiance autocorrelation function due to the irradiance fluctuations $\lambda(\tau)$, where $\lambda(\tau) = \langle \Delta \hat{I}(x, t) \Delta \hat{I}(x, t + \tau) \rangle / \langle \hat{I}(x) \rangle^2$, is related to a normalized excess rate, $\xi(\tau)$, at which TAC conversions are produced by the integral equation [Eq. (3a) in Ref. 6]:

$$\lambda(\tau) = \frac{1}{\theta_1 \theta_2} \xi(\tau) + R_1 \int_{\tau}^{\tau+T_W} \lambda(\tau') d\tau' + R_2 \frac{\theta_2}{\theta_1} \int_0^{\tau+T_L} \lambda(\tau') d\tau' + R_1(\theta_1/\theta_2) \int_0^{T_W} \lambda(\tau') d\tau' + R_2 \int_{-T_L}^{\tau} \lambda(\tau') d\tau'. \quad (3)$$

$\xi(\tau)$ is defined as the actual rate at which TAC conversions are produced minus the rate at which TAC conversions are produced by a field with no correlated irradiance fluctuations divided by the TAC conversion rate for a field with no correlated irradiance fluctuations. R_1 and R_2 are the photodetector average counting rates, and θ_1, θ_2 are dark current counting rate correction factors. T_W is the TAC conversion range and T_L the delay introduced preceding the stop channel of the TAC.

Measurements to determine the structure of $\xi(\tau)$ were made on both a single mode laser and a laser oscillating in two inde-

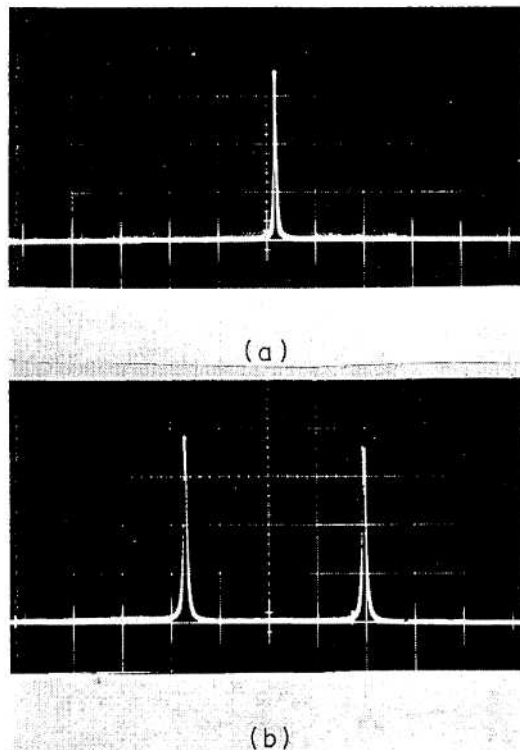


Fig. 2. Optical spectrum analyzer display of output of a He:Ne laser: (a) single mode regime, (b) two mode regime. Dispersion 200 MHz/div.

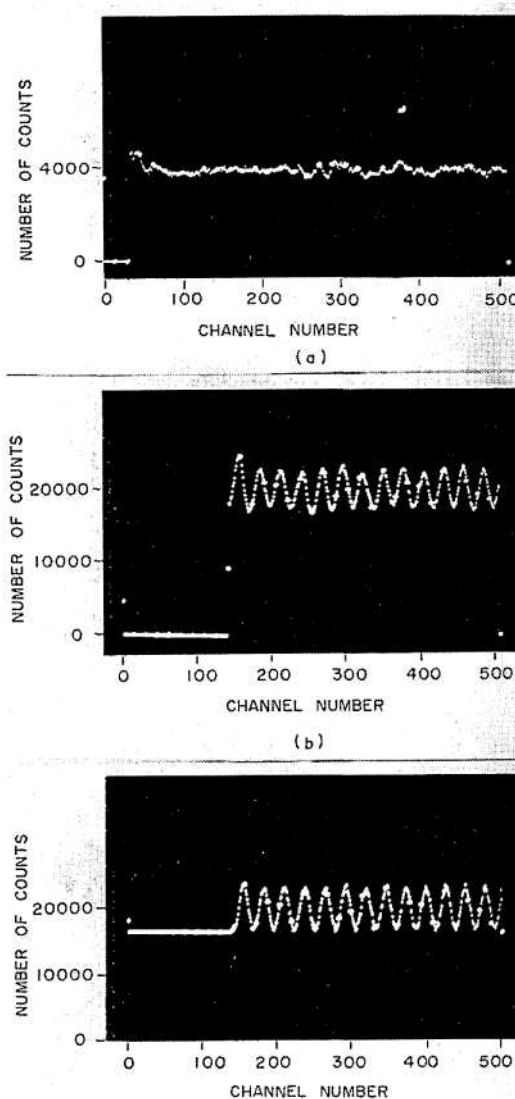


Fig. 3. Pulse height analyzer display of recorded TAC conversions for (a) single mode laser source, (b) two mode laser source, (c) two mode laser source corrected for instrumental response. [100 psec/ch; true zero: channel 160.]

pendent axial modes. Measurements on the single mode laser were used as a check on the apparatus. Since the optical field of a single mode laser has no correlated irradiance fluctuations it should yield the result $\xi(\tau) = 0$ for all τ . The axial mode structure present in the laser beam was measured with a scanning Fabry-Perot interferometer and is shown in Figs. 2(a) and 2(b). The data accumulated in the pulse height analyzer for the two measurements is shown in Fig. 3. All measurements were made with a TAC conversion range of 50 nsec and photodetector average counting rate of 2×10^5 counts/sec. The total counting time was 4.7×10^3 sec, and the TAC deadtime was 6×10^{-6} sec. The irregularities in Figs. 3(a) and 3(b) are due to nonlinearities present in the TAC and do not represent irradiance fluctuation correlations. Figure 3(c) shows the data taken for a two mode laser but corrected for the TAC nonlinearities. The data were obtained by accumulation of 20,000 TAC conversions per channel from the two mode laser, and then subsequent accumulations of conversions in the PHA subtract mode from a single mode laser.

The integral equation for $\lambda(\tau)$ is solved by an iterative procedure, in which the measured quantity $\xi(\tau)$ is taken as the zeroth order solution for $\lambda(\tau)$. The contribution of the integrals on the right-hand side of Eq. (3) is of the order 10^{-3} for the values of R and $(\omega_2 - \omega_1)$ used in the experiment. The dark current correction factors were very nearly 1, since the photodetectors were cooled to a sufficiently low temperature that their dark current counting rates were less than 50 counts/sec. Under the above conditions, $\lambda(\tau) \simeq \xi(\tau)$.

The results of the measurements on the laser oscillating in two independent axial modes yield the following for $\xi(\tau)$: $\xi(\tau) = 0.13 \cos 2\pi 3.70 \times 10^8 \tau$ corresponding to an average period of 27 channels.

The theoretically expected behavior of $\lambda(\tau)$ is given by

$$\lambda(\tau) = \frac{1}{2} e^{-D(\tau)} \cos(\omega_2 - \omega_1)\tau.$$

For the laser investigated, $\omega_2 - \omega_1 = 2\pi 3.70 \times 10^8 \text{ Hz}$, $D < 1 \times 10^6 \text{ sec}^{-1}$, and the mode amplitudes differed by at most 20%. The difference in mode amplitudes reduced $\lambda(\tau = 0)$ to a maximum theoretical value of 0.49. Instead, the discrepancy between the observed maximum value of $\xi(\tau)$ and the maximum excess rate at which conversions are stored in any one channel of the analyzer is mainly due to the time slewing of the photodetectors, pulse amplifiers and discriminators. Measurements of the finite resolution time of the photon counting system yielded a value of 0.68×10^{-9} seconds. Finally we verified that the effect of the spread in transit time of the photoelectrons is in fact of such magnitude as to be responsible for the observed reduction of the theoretical cosine modulation index by assuming a gaussian system function and its convolution with $\xi(\tau)$ (Ref. 7.).

The results of these measurements of the irradiance auto-correlation function in the time domain are in good agreement with comparable measurements in the frequency domain and also with conditional counting probability measurements of Arecchi *et al.*⁸ Frequency analysis of the fluctuating component of a photodetector analog signal yielded a value of 380.45 MHz for the frequency separation between the two axial modes. The period of oscillation of the component of the irradiance auto-correlation function due to the correlated irradiance fluctuations yielded a value of $370 \text{ MHz} \pm 15 \text{ MHz}$ for the frequency separation between the two axial modes. The accuracy is limited by the time resolution of the Ortec model 437A TAC, which is $10p \text{ sec}$ on the $50n \text{ sec}$ conversion range. Measurements of the mode linewidth with the use of a spectrum analyzer yielded a value of the phase diffusion constant, $D < 10^6 \text{ sec}^{-1}$; this is consistent with the negligible decrease in the depth of modulation observed for τ values up to about $40 \times 10^{-9} \text{ sec}$.

While measurements of irradiance correlation functions can, in principle, be used to determine the mode structure and degree of phase locking of a laser beam, the complexity of the correlation functions limits the usefulness of this technique to cases where the mode structure is simple (less than four modes present in the beam). Also the maximum value of the axial mode separation frequency that can be resolved effectively is about 1 GHz equivalent to a period of 9 PHA channels.

However, irradiance correlation function measurements can be successfully made on weak optical fields, whereas considerable difficulty is encountered in the performance of equivalent measurements on weak fields with frequency analysis techniques. The measurements described were performed on an optical field of mean irradiance of the order of 10^{-12} W . These techniques are now being applied to analyze weak fields produced by optical nonlinear processes.⁹

This research was jointly sponsored by ONR under project THEMIS and by a NASA Research grant NSG-6-59.

References

1. L. Mandel and F. Davidson, J. Appl. Phys. **39**, 62 (1968).
2. L. Mandel, in *Proceedings of Symposium on Modern Optics* (Polytechnic Press, Brooklyn, 1967) p. 143.
3. M. Bertolotti, B. Crosignani, P. DiPorto, and D. Sette, Phys. Rev. **150**, 1054 (1966).
4. W. E. Lamb, Jr., *Quantum Optics and Electronics* (Gordon and Breach, New York, 1964) p. 337.
5. L. Mandel and E. Wolf, Rev. Mod. Phys. **37**, 231 (1965).
6. F. Davidson, Phys. Rev. **185**, 446 (1969).
7. A. Papoulis, *System and Transforms with Applications in Optics* (McGraw, Hill, New York, 1968).
8. F. T. Arecchi, E. Gatti, and A. Sona, Phys. Letters **20**, 27 (1966).
9. F. Davidson, J. Klebba, and F. Tittel, Appl. Phys. Letters **17**, 117 (1970).

The Increase of Bragg Diffraction Intensity Due to Acoustic Resonance and Its Application for Demultiplexing and Multiplexing in Laser Communication

C. S. Tsai

Department of Electrical Engineering, Carnegie-Mellon University, Pittsburgh, Pennsylvania 15213.

Received 18 May 1970.

Work on laser-acoustic Bragg diffraction and its applications have been reported frequently in recent years.¹ In much of the work reported, a traveling acoustic wave was used. A standing acoustic wave has also been utilized for laser Q-switching,² mode locking,³ and frequency shifting.⁴ To our knowledge, however, calculation of the increase of the Bragg diffracted light intensity from a standing acoustic wave, because of acoustic resonance, over the Bragg diffracted light intensity from a traveling acoustic wave, has not been reported in the journals.⁵

The purposes of this Letter are to report the results of an analysis for this increase in the diffracted light intensity, and to propose a new application using standing acoustic waves, namely, the demultiplexing and multiplexing devices for a multichannel pulse code modulation (PCM) laser communication system.

Consider an attenuating longitudinal acoustic beam of unit cross-sectional area, propagating along the principle axis of a crystal rod of length L . Both end faces of the rod are clamped mechanically (Fig. 1). We shall designate the acoustic power attenuation constant as 2α nepers per unit length and the power reflection coefficients of the input and output end faces as R_1 and R_2 , respectively. Impedance mismatch at the end faces of the rod results in multiple acoustic reflections and consequently a standing wave. The acoustic strain associated with the standing wave

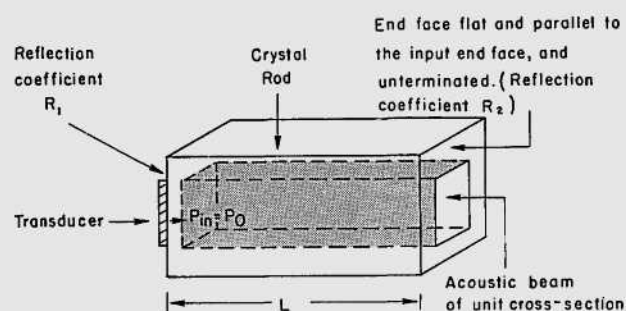


Fig. 1. Geometry of a resonating acoustic beam.